

bradscholars

Structure evolution and orientation mechanism of long-chain-branched poly (lactic acid) in the process of solid die drawing

Item Type	Article
Authors	Li, J.;Li, Z.;Ye, L.;Zhao, X.;Coates, Philip D.;Caton-Rose, Philip D.
Citation	Li J, Li Z, Ye L et al (2017) Structure evolution and orientation mechanism of long-chain-branched poly (lactic acid) in the process of solid die drawing. European Polymer Journal. 90: 54-65.
DOI	https://doi.org/10.1016/j.eurpolymj.2017.03.005
Rights	© 2017 Elsevier. Reproduced in accordance with the publisher's self-archiving policy. This manuscript version is made available under the CC-BY-NC-ND license (https://creativecommons.org/licenses/by-nc-nd/4.0/)
Download date	2026-06-09 00:07:09
Link to Item	http://hdl.handle.net/10454/17003

**Structure Evolution and Orientation Mechanism of
Long-Chain-Branched Poly (lactic acid) in the Process of Solid Die
Drawing**

¹Jiafeng Li, ¹Zhengqiu Li, ¹Lin Ye, ¹Xiaowen Zhao*, ²Phil Coates, ²Fin Caton-Rose,
²Michael Martyn

1. State Key Laboratory of Polymer Materials Engineering of China, Polymer Research
Institute of Sichuan University, Chengdu, China
2. School of Engineering, Design and Technology, University of Bradford, Bradford, U.K.

*Corresponding author. Tel.: 862885408802; Fax: 862885402465. E-mail address:

zhaoxiaowenscu@126.com

Abstract: Highly oriented long-chain-branched poly (lactic acid) (LCB-PLA) was prepared and the structure evolution was studied in the process of solid die drawing by compared with poly (lactic acid) (PLA). During drawing, samples underwent not only die drawing process but also free drawing process. Drawing speed presented a prominent effect on the free drawing process, while die thickness showed a more obvious influence on the die drawing process. For PLA, free drawing process mainly contributed to its final orientation degree and crystallinity, and thus the mechanical properties of PLA were greatly influenced by drawing speed. However, for LCB-PLA, die drawing process made a greater contribution to the final orientation degree and crystallinity, and its mechanical properties were mainly affected by die thickness. Under the same drawing condition, the tensile strength and modulus of LCB-PLA were always higher than those of PLA, and reached up to 228 MPa and 7.2 GPa, respectively, which basically met the requirement for born fixation materials. Samples which only underwent die drawing showed obvious “sandwich” structure, and the thickness of the oriented skin layer for LCB-PLA was thicker than that for PLA, suggesting that shear-induced orientation can be easily retained due to the enhanced entanglement between long branched chains. After drawing, LCB-PLA samples showed smaller lamellae size (L_{lateral}) but larger long period (L_{ac}) compared with PLA, suggesting that the low chain mobility restricted the motion of chain slipping of LCB-PLA and thus resulted in the fragmentation of neighboring crystal lamella by chain stretched-out.

Keywords: long chain branched poly (lactic acid) (LCB-PLA); solid die drawing; structure evolution; orientation mechanism

1. Introduction

Poly (lactic acid) (PLA, $-\text{[CH}(\text{CH}_3)\text{COO}]_n-$), a linear aliphatic thermoplastic polyester which is produced from lactic acid by converting sugar or starch obtained from renewable

sources (e.g., corn, wheat, or rice), has been a focus of research during recent decades because of its potential applications in the fields of biomedical products [1]. But the brittleness and unsatisfied mechanical strength of PLA greatly limit its wide applications as bone screws, bone fixation plate, stent and so on.

Molecular orientation can greatly improve the mechanical and physical properties of PLA. Long Yu et al. produced two types of oriented PLA films (one amorphous and one semi-crystalline) by using an extruder and sheet die [2]. The maximum draw ratio was 200%, and the tensile strength and modulus can reach up to 121.1MPa and 3.9GPa respectively. Yuan et al. fabricated PLLA fibers through a two-step melt-spinning method (melt extrusion and hot drawing) [3]. During the hot drawing process, the maximum draw ratio of 589% and tensile modulus of 3.6–5.4 GPa were obtained for the fiber. PLA fiber was also prepared by Bhuvanesh Gupta et al. by using dry-jet-wet spinning method [4]. The draw ratio plays an important role in the structural development of the fiber and the maximum draw ratio of 1000% was achieved. Anyway, due to the very low viscosity and low melt strength of PLA, ultra-drawing and high orientation for PLA is very difficult, and thus the enhancement of the mechanical property through molecular orientation is limited.

Solid die drawing is an effective way to obtain molecular orientation for polymer in solid phase. During this process, a billet of polymer is heated to a temperature below its melting point before drawn through a fixed shape die by an axial load. Then the billet is constrained to follow the shape of the die, which has a reduced cross section, and therefore it undergoes axial extension. When the billet is drawn out of the die exit, the material also undergoes free drawing and further axial extension of the material occurs. Compared with other orientation processes, such as free solid drawing [5,6] and electrospinning [7,8], through solid die drawing process, not only high production rates and high orientation can be achieved without complex processing apparatus, but thick section samples including tubes, tapes, etc. can also be

produced [9,10]. Although the development of the die drawing process on polyolefin is highly successful, die drawing of PLA and its structure evolution during the process have been scarcely reported.

In our previous study, in order to enhance the melt strength and thus obtain high orientation degree, long-chain-branched PLA (LCB-PLA) was prepared through a two-step ring-opening reaction with anhydride and epoxy during processing [11]. The topological structure of LCB-PLA was made of linear chains, star-like chains with three arms and tree-like chains with two generations, and during hot stretching, the maximum draw ratio as high as 1200% can be achieved [12]. Because the molecular entanglements play a key role in shear-/strain-induced orientation and crystallization, the unique molecular architecture of the LCB-PLA provides an opportunity to study its effects on the processing-induced orientation and structure developments.

In this study, highly oriented PLA and LCB-PLA were prepared through solid die drawing technology. The influence of drawing conditions, such as the die thickness and drawing speed, on the microstructure and mechanical properties of LCB-PLA was studied in comparison with PLA. During solid die drawing, sample can be divided into three distinct zones as shown in Fig.1, including undeformed part (Region I), the part which deformed within the die (Region II) and the part drawn out of the die where a substantial free drawing can occur (Region III). Because the structure evolution of sample was quite different in the above mentioned three regions, it is necessary to discriminate the contributions of die drawing and free drawing outside the die to the formation of oriented structure of LCB-PLA and PLA during die drawing processing.

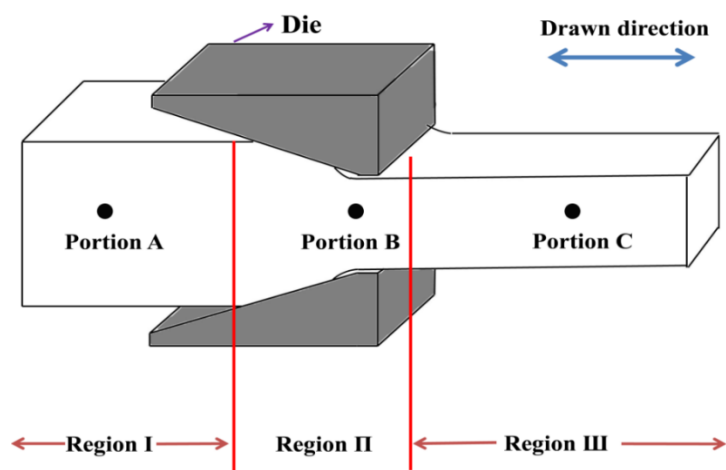


Fig. 1 Schematic diagram of PLA samples drawn through a die

2. Experimental section

2.1 Materials

Poly (lactic acid) (PLA) (NatureWorks® PLA Polymer 3052D) was supplied by Nature Works Co., USA. The molecular weight (M_w) was about 1×10^5 and the molecular weight distribution index (M_w/M_n) was about 1.21. Pyromellitic dianhydride (PMDA)(AR) was obtained from Sinopharm Chemical Reagent Co. Ltd, China. Pentaerythritol polyglycidyl ether (PGE) (AR) was obtained from Energy Chemical Reagent Co. Ltd, China.

2.2 Preparation of highly oriented LCB-PLA

LCB-PLA was prepared according to our previous work. After dried at 70 °C for 5hrs in a vacuum oven, PLA pellets were added in a Haake internal melt mixer (Rheocord 90, Germany) at 180 °C. When they were totally melted, PMDA was added to react with PLA for several minutes, and then PGE was added into the mixture. After mixing for about 50 min, the reaction was completed and the product was cut into small granules.

Highly oriented LCB-PLA were prepared by using die-drawing apparatus as shown schematically in Fig.2. It consisted of three parts including preheater, converging die and drawing devices. At first, LCB-PLA billets were placed in the preheater and maintained at 85 C for a certain time to establish thermal equilibrium. Then billets were drawn through the die

under different die thickness (0.55mm, 0.75mm, 1mm, 2mm) and drawing speed (62.5mm/min, 250mm/min, 500mm/min, 1000mm/min). Finally, the obtained oriented samples were cooled down while remaining in the die under load.

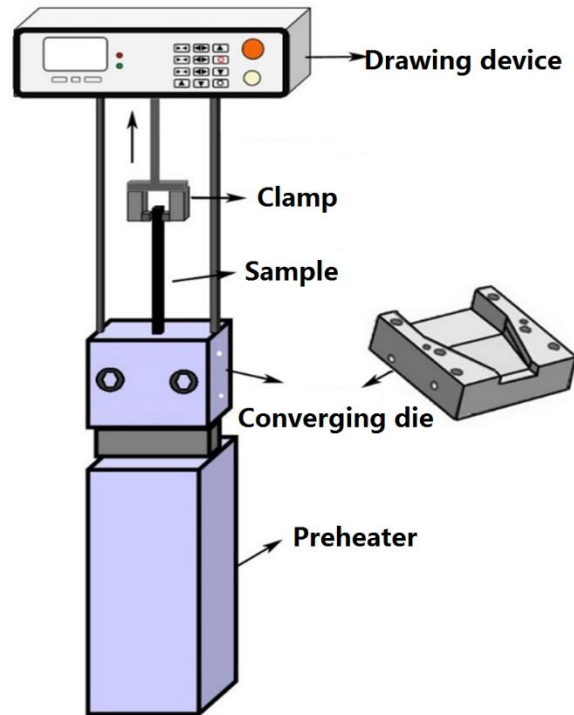


Fig. 2 Schematic diagram of the die-drawing machine

2.3 Measurements

2.3.1 Two-dimensional wide-angle X-ray diffraction analysis (2D-WAXD)

Two-dimensional wide-angle X-ray diffraction analysis of PLA samples was conducted at the ambient temperature using a D8 Discover two-dimensional wide angle X-ray diffractometer (2D-WAXD) (Bruker AXS Co., Germany). The sampling time of 2D-WAXD measurements was 180 s using an Eulerian 1/4 cradle HI-STAR (2D-Detector) detector and the wavelength was 0.154 nm.

2.3.2 Two-dimensional small-angle X-ray scattering analysis (2D-SAXS)

Two-dimensional small-angle X-ray scattering analysis of PLA samples was performed at the beam line BL16B1 of Shanghai Synchrotron Radiation Facility with a sample-detector distance of 1866 mm using Cu ($K\alpha$) radiation ($\lambda= 1.24\text{\AA}$) and a $2 \times 2 \text{ cm}^2$ area detector. Data

processing was performed with the software “Fit2D 2012”. The SAXS patterns were normalized to the primary beam intensity and corrected for background scattering.

2.3.3 Non-isothermal crystallization analysis

The non-isothermal crystallization of PLA samples was performed with a Netzsch 204 differential scanning calorimetry (DSC) (Phoenix Co, Germany). The temperature scale of DSC was calibrated with indium. Granulated samples of about 10 mg were heated from ambient temperature to 200 °C at a constant rate of 10 K/min under nitrogen atmosphere. X_c can be calculated with the following equation [13]:

$$X_c = (\Delta H_m / \Delta H_0) \cdot 100\% \quad (1)$$

where ΔH_m and ΔH_0 was the melting enthalpies for the samples and the 100% crystalline PLA, respectively. ΔH_0 was considered to be 93J/g. An overall accuracy of 0.5°C in temperature and 1% in enthalpy was estimated.

2.3.4 Mechanical properties

The mechanical properties of PLA and LCB-PLA samples were measured by Instron 4302 material testing machine (Instron Co., USA) according to ISO527-1-2012(E) [14]. The test speed was 50 mm/min, and the sample length between benchmarks was 15 mm. All the values presented were the average of five specimens.

2.3.5 Scanning electron microscope analysis (SEM)

The fractured surface morphology analysis of PLA samples was performed with JEOL JSM-5900LV scanning electron microscope (JEOL co, Japan) with an acceleration voltage of 5 kV.

3. Results and Discussion

During die drawing, the structure and properties of PLA and LCB-PLA samples at three portions along the drawing direction (Fig. 1) were studied. At Portion A (in Region I), the sample was moving towards the die entrance and deformation had not begun yet, while, at

Portion B (in Region II), the sample had been just drawn out of the exit of the die at processing temperature and underwent just die drawing. Portion C (in Region III) was located at a distance of about 100 mm from the exit of the die, where sample was cooled completely and underwent not only die drawing but also free drawing. Therefore, the orientation factor and crystallinity of the final obtained sample in this study can be described as:

$$X_{\text{final}} = X_{\text{die}} + X_{\text{free}} \quad (2)$$

$$F_{\text{final}} = F_{\text{die}} + F_{\text{free}} \quad (3)$$

where, X_{final} and F_{final} were the final crystallinity and final orientation factor of the sample respectively, which were determined by the sample located at Portion C; X_{die} and F_{die} were the crystallinity and orientation factor of the sample just suffer die drawing, which were determined by the sample located at Portion B; X_{free} and F_{free} were the crystallinity and orientation factor of the sample just suffering free drawing outside the die.

3.1 Effect of drawing speed on the orientation structure and crystalline behavior of LCB-PLA

Orientation structure

The effect of drawing speed on the orientation structure of LCB-PLA was studied by compared with PLA and the 2D-WAXD patterns for samples produced under die thickness of 0.55mm and varying drawing speed were shown in Fig. 3. For samples at Portion A, diffraction patterns of both PLA and LCB-PLA did not show any Debye-Scherrer diffraction rings due to the low crystallinity and the random arrangement of grains. For samples at Portion B, two weak circular spots on the equator of (200)/(110) reflection can be observed for both PLA and LCB-PLA samples indicating the preferred orientation of PLA chains along drawing direction. Moreover, at this Portion, a four-point image of (203) reflection formed in LCB-PLA samples, which cannot be observed for PLA sample, suggesting a higher orientation degree and crystallinity for LCB-PLA sample at Portion B. However, at Portion C, the two strong circular

spots on the (200)/(110) reflection equator and the four-point image of (203) reflection can be observed for both PLA and LCB-PLA.

With the increase of drawing speed, these diffraction arcs became narrower in spread and more prominent indicating that the crystal orientation increased. At high drawing speed above 500mm/min, the apparent (116) reflections exhibited isosbestic points for both PLA and LCB-PLA. θ

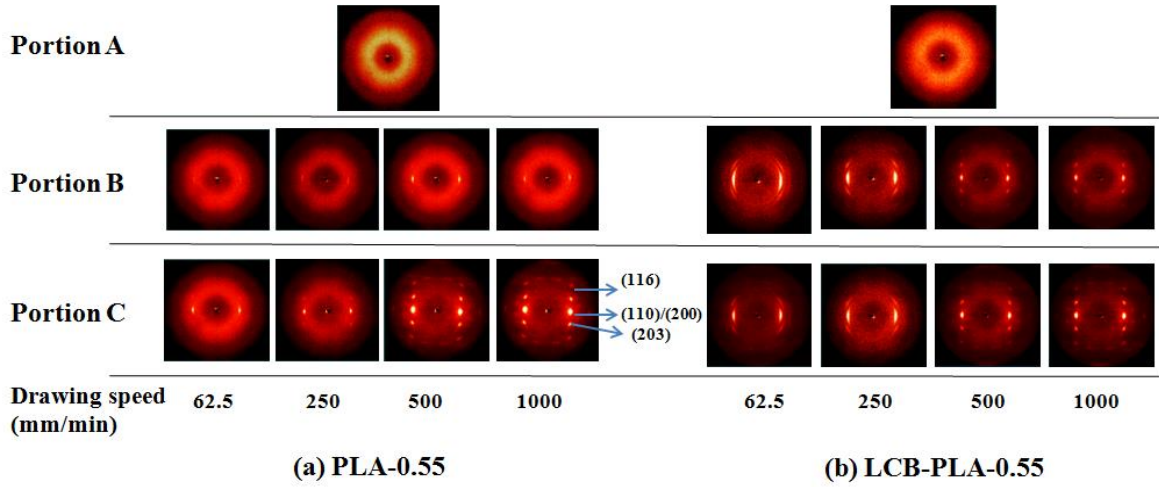


Fig. 3 2D-WXRD patterns of (a) PLA and (b) LCB-PLA drawn under different drawing speed and die thickness of 0.55mm

The orientation factor (F) was calculated using Herman's orientation function [15, 16]:

$$F = \frac{3\langle \cos^2 \phi \rangle - 1}{2} \quad (4)$$

$$\langle \cos^2 \phi \rangle = \frac{\int_0^{\pi/2} I(\phi) \sin \phi \cos^2 \phi d\phi}{\int_0^{\pi/2} I(\phi) \sin \phi d\phi} \quad (5)$$

where $I(\Phi)$ is the scattering intensity along the angle Φ . When the crystals are oriented with the direction parallel to the reference axis, $F=1$; when the crystals are oriented with the direction perpendicular to the reference axis, $F= -0.5$, and for random orientation, $F = 0$.

Orientation factors of PLA and LCB-PLA drawn under different drawing speed were calculated with Equation (4) and (5), as shown in Fig. 4. At portion A, the lamellae of PLA and LCB-PLA samples were randomly arranged and the orientation factor nearly approached 0. At portion B, the orientation degree of PLA samples at different drawing speed was very low

because of the “weak” orientation, however, the orientation factors of LCB-PLA samples were much higher than that of PLA due to the “strong” orientation induced by the die. At portion C, the orientation factor of both PLA and LCB-PLA samples can approach relatively high value, due to the regular and preferential orientation. In order to distinguish the effect of die drawing and free drawing on the orientation structure of LCB-PLA, the orientation factors contributed by free drawing (F_{free}), were also calculated with Equation (2). As shown in Fig. 4, it was noteworthy that, for PLA, F_{free} was much higher than F_{die} at the same drawing speed, while for LCB-PLA, F_{free} was much lower than F_{die} , demonstrating that, for PLA, the free drawing process mainly contributed to its final orientation degree, but for LCB-PLA, die drawing process made a greater contribution to the final orientation degree.

In addition, it can be observed from Fig. 4 that, with increasing drawing speed, the final orientation factor (samples located at Portion C) increased significantly for PLA but nearly maintained constant for LCB-PLA, suggesting that drawing speed presented a more prominent effect on the free drawing process and thus the orientation degree of PLA.

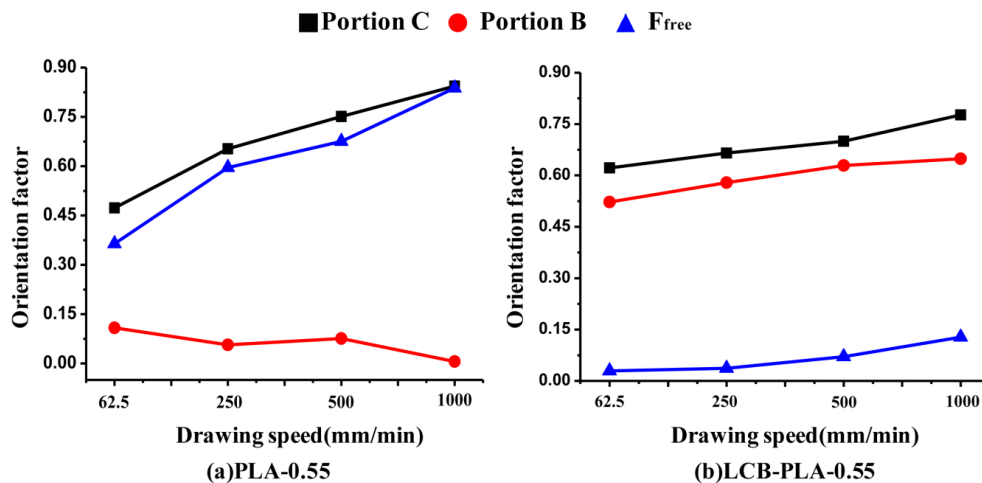


Fig. 4 Orientation factors of PLA and LCB-PLA samples drawn under different drawing speed and die thickness of 0.55mm

Crystalline behavior

The DSC curves of PLA and LCB-PLA drawn under varying drawing speed and constant die thickness were displayed in Fig. 5. The curves of all samples exhibited two distinct peaks

corresponding to glass transition at around 58°C and melting peaks at around 155°C respectively.

Before drawing, the initial crystallinity for both PLA and LCB-PLA was very low, and the melting peaks were mainly induced by cold crystallization behavior when the samples were heated during the measurement. At portion B, exothermic peaks related to cold crystallization behaviors can also be clearly observed for PLA, however, there was no detectable cold crystallization peak for LCB-PLA, suggesting that, at Portion B, crystalline phase were scarce and imperfect for PLA samples but sufficient and perfect for LCB-PLA samples. At portion C, no cold crystallization peak can be observed for both PLA and LCB-PLA samples due to the formation of regular and perfect crystalline structure at this portion.

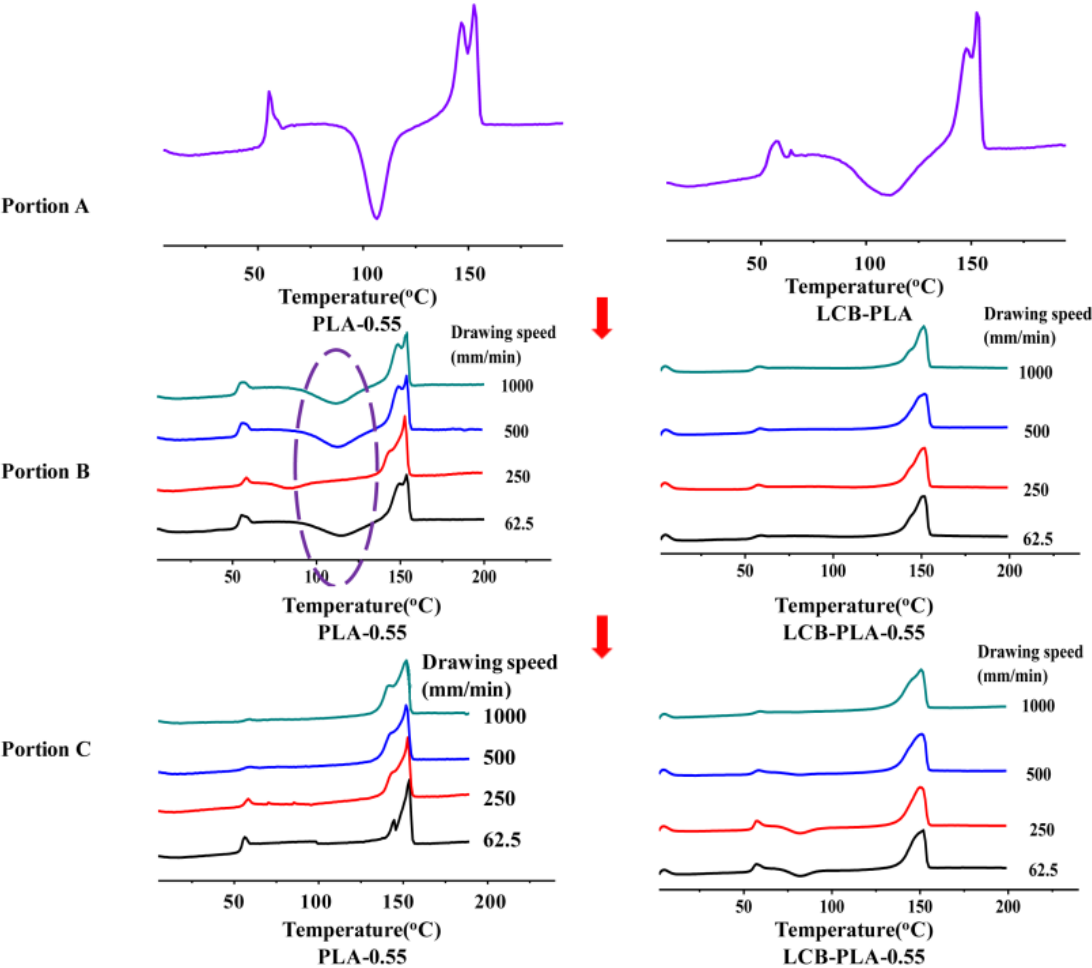


Fig. 5 DSC curves of PLA and LCB-PLA samples drawn under different drawing speed and die thickness of 0.55mm

The crystallinity was calculated and shown in Fig.6. At portion B, the crystallinity of PLA samples was very low, however, the crystallinity of LCB-PLA samples was much higher. At portion C, both PLA and LCB-PLA samples can reach a relatively high crystallinity. In order to distinguish the effects of die drawing process and free drawing process on the crystalline property of LCB-PLA, crystallinity contributed by free drawing process (X_{free}), was calculated with Equation (3). As shown in Fig. 6, it can be seen that, for PLA, X_{free} was higher than X_{die} at the same drawing speed, while for LCB-PLA, X_{free} was much lower than X_{die} , suggesting that free drawing process mainly contributed to the final crystallinity for PLA, but for LCB-PLA, die drawing process mainly contributed to the final crystallinity.

Moreover, with increasing drawing speed, the final the crystallinity (samples located at Portion C) increased significantly for PLA but nearly maintained constant for LCB-PLA, suggesting that drawing speed showed a more prominent effect on free drawing process and the crystallinity of PLA.

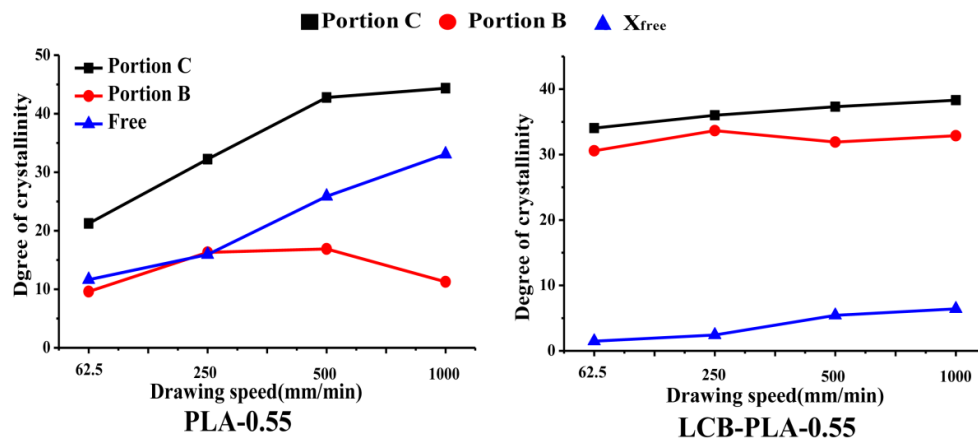


Fig. 6 Crystallinity of PLA and LCB-PLA samples drawn under different drawing speed and die thickness of 0.55mm

3.2 Effect of die thickness on the orientation structure and crystalline behavior of LCB-PLA

Orientation structure

2D-WAXD patterns of PLA and LCB-PLA samples drawn under constant drawing speed of 1000mm/min and different die thickness were shown in Fig. 7. At Portion B, when PLA samples were drawn with thick die (thicker than 0.75mm), no obvious diffraction rings or arcs can be observed due to the low orientation degree and crystallinity. While for LCB-PLA, two weak circular spots on the equator of (200)/(110) reflection can be observed in spite of the die thickness. Moreover, at this portion, a four-point image of (203) reflection formed for LCB-PLA samples drawn with thin die (thinner than 1mm). For samples at Portion C, both the two strong circular spots on the (200)/(110) reflection equator and the strong four-point image of (203) reflection can be observed for PLA and LCB-PLA.

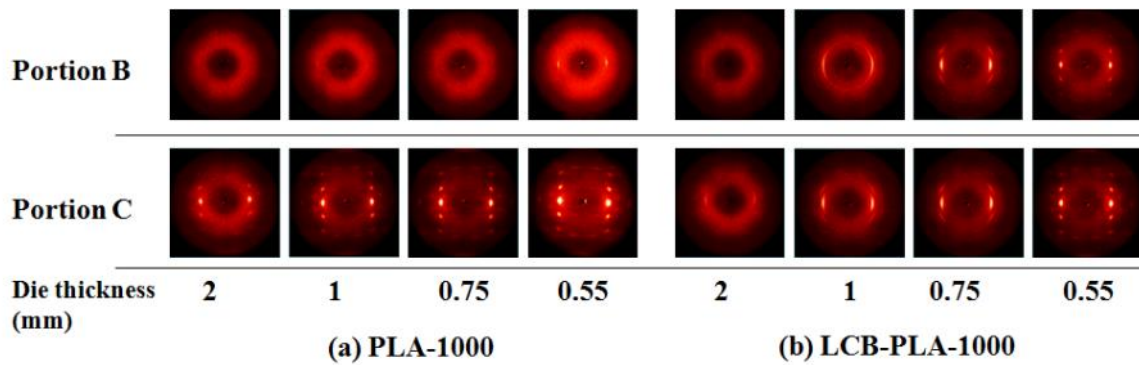


Fig. 7 2D-WXRD patterns of (a) PLA and (b) LCB-PLA drawn with different die thickness and drawing speed of 1000mm/min

Orientation factors of PLA and LCB-PLA produced with different die thickness were calculated as shown in Fig. 8. At portion B, the orientation degree of PLA samples with different die thickness was very low, however, the orientation factors of LCB-PLA samples were much higher and increased gradually with the decrease of die thickness due to the high die-induced orientation for LCB-PLA. At portion C, the orientation factors of both PLA and LCB-PLA samples can reach a relatively high value. For PLA, F_{free} were much higher than F_{die} at the same die thickness, while, for LCB-PLA, F_{free} were much lower than F_{die} .

In addition, it can be observed from Fig. 8 that, with decreasing die thickness, the final orientation factor (Portion C) increased significantly for LCB-PLA but nearly maintained

constant for PLA, suggesting that die thickness showed a more prominent effect on die drawing process and thus the orientation degree of LCB-PLA.

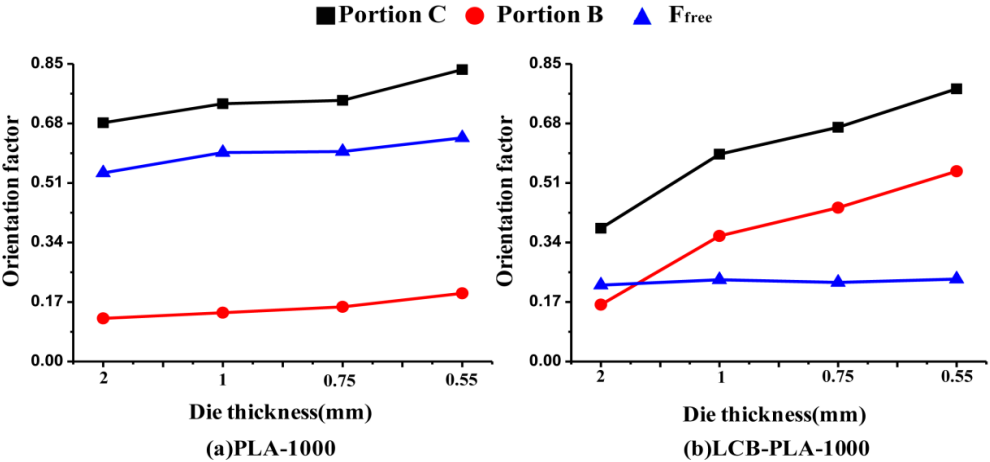


Fig. 8 Orientation factor of PLA and LCB-PLA samples drawn with different die thickness and drawing speed of 1000mm/min

Crystalline behavior

The DSC curves and crystallinity of PLA and LCB-PLA drawn under variable die thickness at different region were displayed in Fig. 9 and Fig. 10, respectively. At portion B, cold crystallization peaks can be observed for PLA samples drawn with different die thickness. However, for LCB-PLA, cold crystallization just can be observed for samples drawn with thick die above die thickness of 1mm, and disappeared when samples were drawn with low die thickness. At portion C, after free drawing, cold crystallization peak cannot be observed for PLA samples because of perfect crystalline structure. However, at this portion, LCB-PLA samples drawn with thick die still showed cold crystallization behavior.

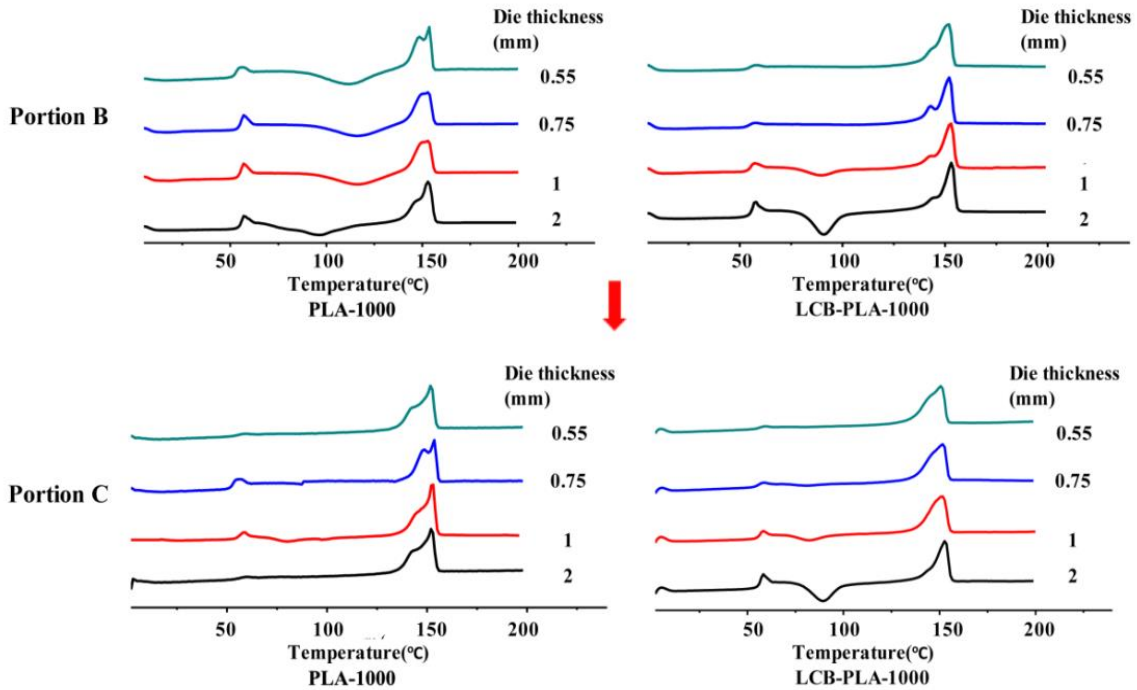


Fig. 9 DSC curves of PLA and LCB-PLA samples drawn with different die thickness and drawing speed of 1000mm/min

The crystallinity was calculated as shown in Fig.10. At portion B, the crystallinity of PLA samples was very low, however, the crystallinity of LCB-PLA samples was much higher. At portion C, the crystallinity for both PLA and LCB-PLA increased obviously compared with samples at Portion B. For PLA, X_{free} was much higher than X_{die} , while, for LCB-PLA, X_{free} was much lower than X_{die} at the same die thickness.

With decreasing die thickness, the final crystallinity (Portion C) increased significantly for LCB-PLA but nearly maintained constant for PLA, suggesting that die thickness may show more dominant effect on die drawing process and thus the crystallinity of LCB-PLA.

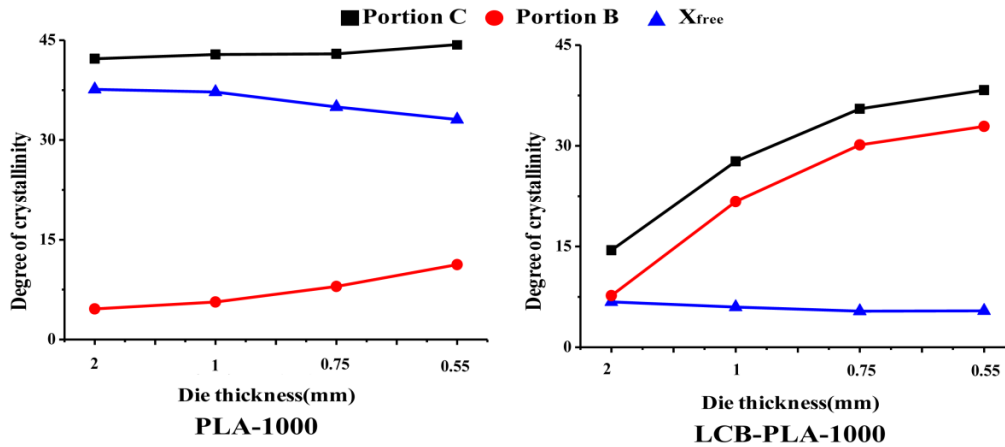


Fig. 10 Crystallinity of PLA and LCB-PLA samples drawn with different die thickness and drawing speed of 1000mm/min

3.3 Mechanical properties of oriented LCB-PLA

The mechanical properties of PLA and LCB-PLA drawn under different conditions were shown in Fig. 11. It can be seen that, after die drawing, the tensile strength and modulus of both PLA and LCB-PLA were enhanced greatly, while the elongation at break decreased slightly. With the increase of drawing speed, the tensile strength of both PLA and LCB-PLA increased gradually. While, with the decrease of die thickness, the strength increased sharply for LCB-PLA, but nearly maintained constant for PLA. Because drawing speed presented a prominent effect on the free drawing process and thus the final orientation degree and crystallinity of PLA, the mechanical properties of PLA were greatly influenced by drawing speed. Likewise, the reason why mechanical properties of LCB-PLA were mainly affected by die thickness can also be explained. Under the same drawing condition, the tensile strength and modulus of LCB-PLA were always higher than those of PLA. At 1000mm/min of drawing speed and 0.55mm of die thickness, the tensile strength and modulus of LCB-PLA reached up to 228 MPa and 7.2 GPa, respectively, which basically met the requirement for born fixation materials.

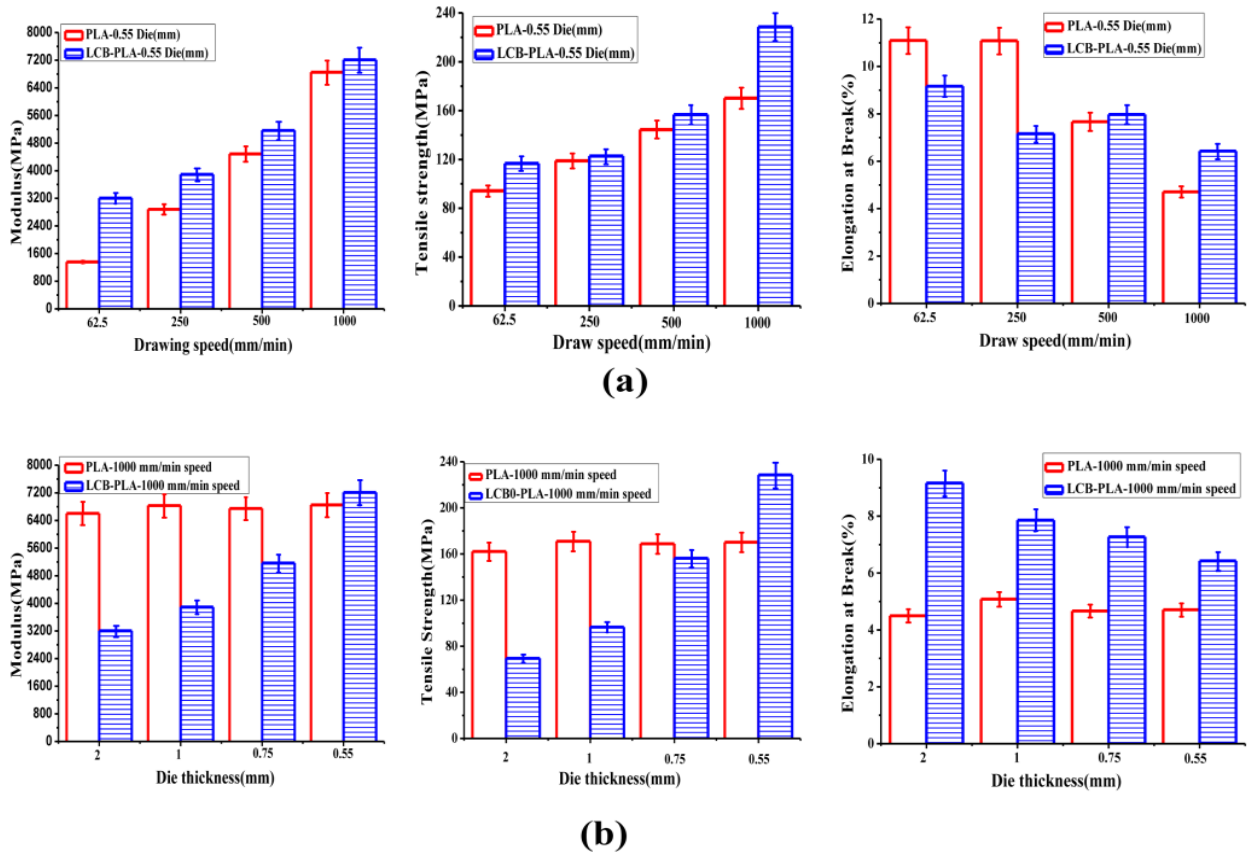


Fig. 11 Mechanical properties of the oriented PLA and LCB-PLA samples (a) Samples drawn under a constant die thickness of 0.55mm and varying drawing speed (b) Samples drawn under a constant drawing speed of 1000mm/min and varying die thickness

3.4 Morphology of oriented LCB-PLA

The section morphology of the oriented PLA and LCB-PLA samples at Portion B and Portion C by drawing at drawing speed of 1000mm/min and die thickness of 0.55mm, was shown in Fig. 12. At Portion B, an obvious “sandwich” structure can be observed for both PLA and LCB-PLA, which showed the highly oriented fibrous morphology in the skin layer and relative low oriented structures in the core layer [17, 18]. When samples went through the convergent die with a constant speed, the velocity was zero at the die wall, which was much slower than that at the center, and thus samples near the surface was stretched by the shear stress while the part of the sample near the center was compressed, resulting in oriented skin layer and isotropic core layer. However, for PLA, the thickness of the oriented skin layer was about 85 μ m, while for LCB-PLA, skin layer was thicker and its thickness reached about 205 μ m,

suggesting that shear-induced orientation was more obvious for LCB-PLA during die drawing process.

At Portion C, both PLA and LCB-PLA exhibited uniform orderly arranged fibrillar bundle structure. When samples were drawn out of the die, the deformation-induced orientation occurred both in skin and core layer of the samples during free drawing process.

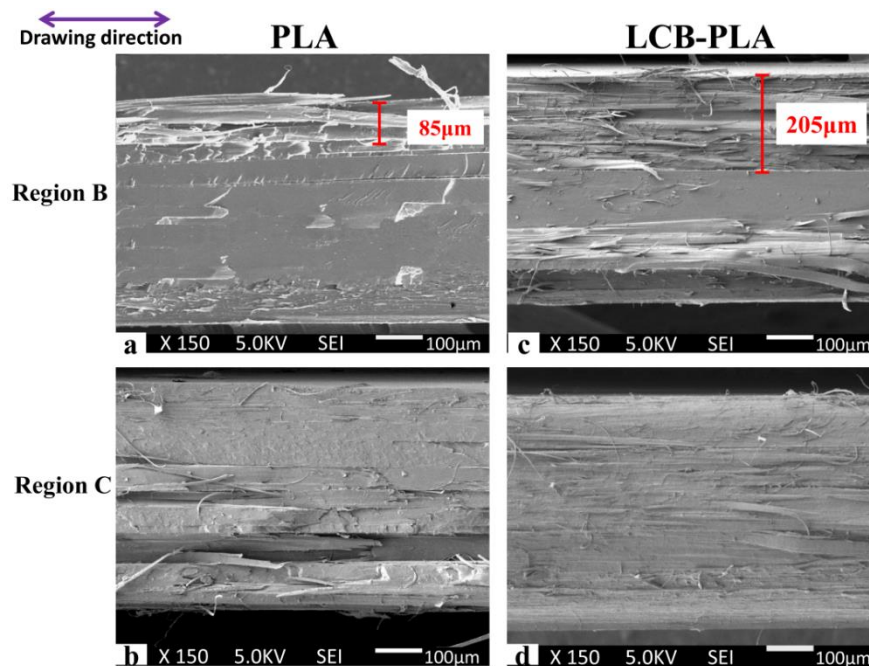


Fig. 12 SEM images of fracture surface for PLA and LCB-PLA during die drawing (Drawing direction was indicated by the arrow)

3.5 Orientation mechanisms of LCB-PLA in the process of solid die drawing

The possible orientation mechanism of PLA and LCB-PLA was schematically shown in Fig.13. Before die drawing, the arrangement of both PLA and LCB-PLA chains were disordered with Gaussian conformation. Then, when samples were drawn through the converging die, they suffered shear stress in the die, and the macromolecular chains were stretched and aligned along drawing direction. However, there existed a competition between chain orientation during shear and relaxation after the removal of shear [19, 20]. For PLA, due to the relatively short and semirigid macromolecular chains, it suffered from undesired fast relaxation after the removal of shear. And consequently, the shear-induced orientation and

crystallization were not easily retained. While for LCB-PLA, the relaxation was restrained due to the enhanced entanglement between long branched chains. Therefore, when the sample of LCB-PLA was drawn through the die, macromolecule chains can be strongly stretched and the stretched chain conformation could be retained, and thus, after the removal of shear (when sample was drawn out of the die), high orientation degree and crystallinity of the LCB-PLA sample can be obtained.

During the free drawing process, for PLA, the weak entanglement between macromolecular chains reduced the constraints for motions of the folded chain crystallization and inter-lamellar coiled segments, and thus the orientation degree and crystallinity increased remarkably during this deformation stage. While for LCB-PLA, the high entanglement density and poor chain mobility would restrict the motion of chain slipping, which may seriously hinder reaching a high degree of orientation and crystallization during this stage.

Therefore, during die drawing, for LCB-PLA, its orientation degree and crystallinity were mainly determined by the die drawing process, while for PLA, the orientation degree and crystallinity were mainly determined by the free drawing process.

In order to find out the final crystalline and oriented structure of PLA and LCB-PLA after drawing, the 2D-SAXS of the both samples were compared, as shown in Fig. 13. It was seen that, the initial isotropic scattering ring in the SAXS pattern became two bar like on the meridian after drawing. The two-bar SAXS pattern on the meridian indicated two possible cases: (1) The “original” lamellar stacks parallel to the stretching direction were destroyed to form new lamellae perpendicular to the stretching direction. (2) The “original” lamellar stacks perpendicular to the stretching direction became fragmented and reorganized to form close stacking.

In order to obtain more detailed information, the structural parameters of lamellae were discussed. The scattering vectors along and perpendicular to the stretching direction were

defined as q_x and q_y as shown in the upper left corner of Fig. 13(a). The size of the lamellae (L_{lateral}) can be derived from the scattering intensity distribution ($I(q_y)$) along the q_y direction. The curves of $I(q_y)$ were fitted with Lorentz functions as the blue and green lines shown in Fig.13(a). The width of the resulting Lorentz function Δq_y (the width of the peak at half height of the blue curve) was related to the L_{lateral} according to $L_{\text{lateral}} = 2\pi/\Delta q_y$ [21]. It can be seen that, the average L_{lateral} of PLA was much larger than that of LCB-PLA (as shown in Fig.13(c)). It was the evidence that less crystal fragmentation occurred for PLA after drawing.

The long period (L_{ac}) of lamellar along the stretching direction of the samples can be obtained by considering the scattering intensity distribution along the q_x direction $I(q_x)$. Then L_{ac} can be calculated from the peak position of $I(q_x)$ according to Bragg's law [22]:

$$L_{\text{ac}} = 2\pi/q_{x \text{ max}}$$

The profiles of $I(q_x)$ of PLA and LCB-PLA were shown as Fig.13(b). It can be seen that, the average long period (L_{ac}) along the stretching direction for PLA was much smaller than that of LCB-PLA, attributed to the newly formed lamellae in amorphous region between existing ones for PLA after drawing. Due to the weak entanglement, the folded-chain crystals of PLA can form easily from inter-lamellar coiled segments during deformation. While for LCB-PLA, the poor chain mobility would restrict the motion of chain slipping and thus result in the fragmentation of neighboring crystal lamella by chain stretched -out. The stretched-out chains can be transformed into the oriented mesomorphic phase (colored in yellow, right diagram of Fig. 14) during drawing, presenting extended-chain conformation without regular helix conformation as in the crystal lamellae [23, 24].

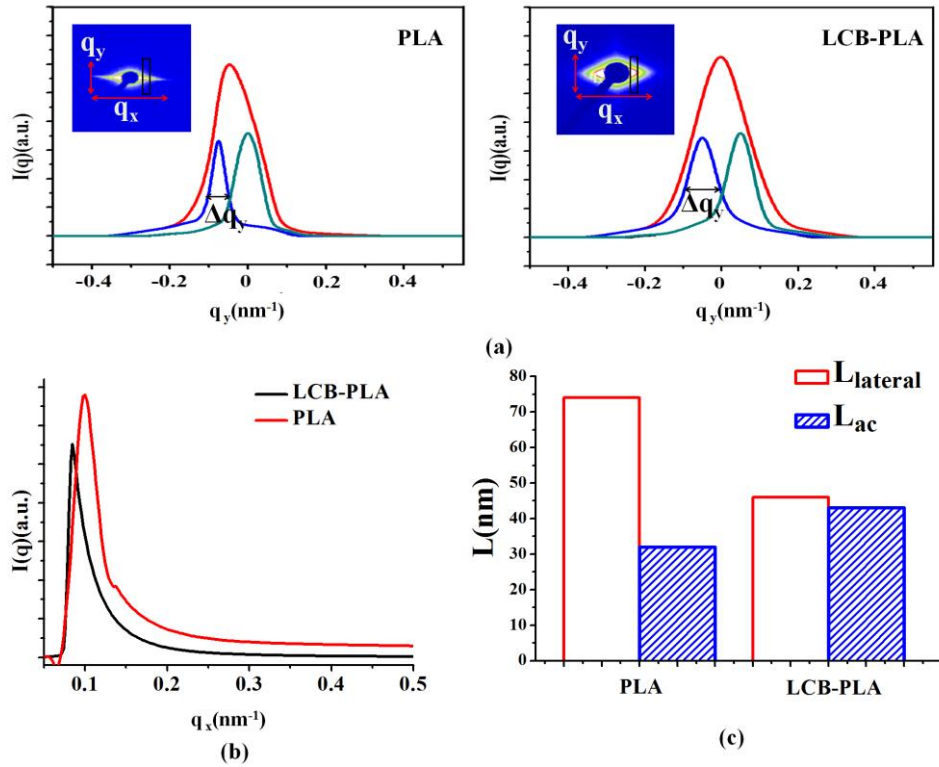


Fig. 13 (a) The azimuthal scan of the lamellar peaks along q_y , (b) The one-dimensional scattering intensity distribution along q_x , (c) The average value of $L_{lateral}$ and L_{ac} of PLA and LCB-PLA

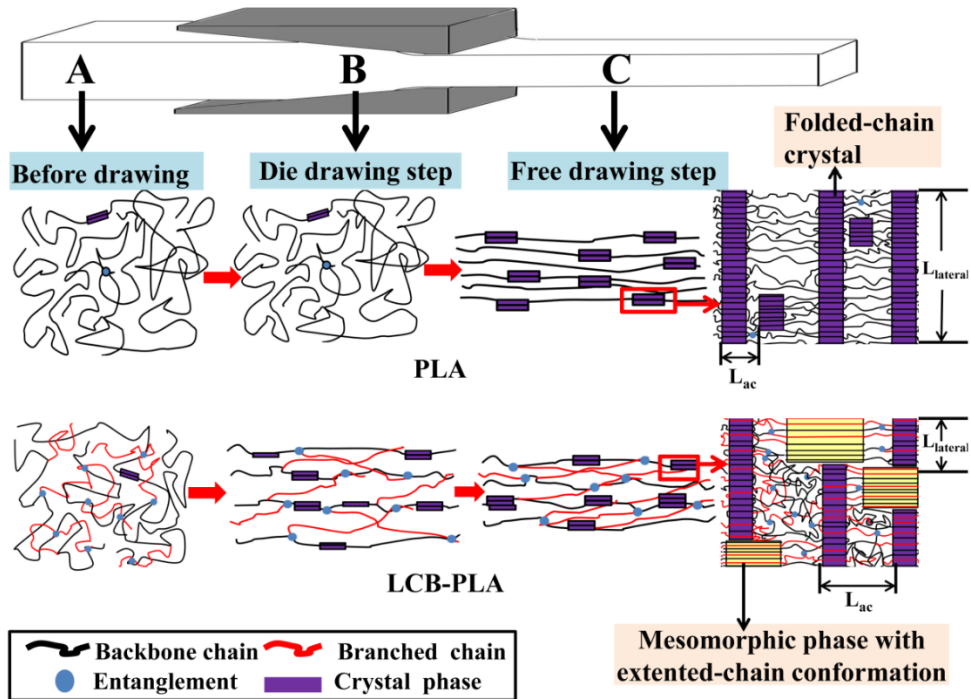


Fig. 14 Proposed morphology evolution of PLA and LCB-PLA during solid die drawing process

4. Conclusions

Highly oriented LCB-PLA were prepared through solid die drawing technology and the influence of drawing conditions on the microstructure and mechanical properties of LCB-PLA was studied in comparison with PLA. Drawing speed presented a prominent effect on the free drawing process, while die thickness showed a more obvious influence on the die drawing process. For PLA, free drawing process mainly contributed to its final orientation degree and crystallinity, and thus the mechanical properties of PLA were greatly influenced by drawing speed. However, for LCB-PLA, die drawing process made a greater contribution to the final orientation degree and crystallinity, and its mechanical properties were mainly affected by die thickness. After drawing, the tensile strength and modulus of LCB-PLA can reach up to 228 MPa and 7.2 GPa respectively, which basically met the requirement for born fixation materials. The morphology of samples which only underwent die drawing showed obvious “sandwich” structure, and the thickness of the oriented skin layer for LCB-PLA was much thicker than that of PLA, suggesting that shear-induced orientation can be retained to a larger extent due to the enhanced entanglement between long branched chains. Under the same drawing condition, LCB-PLA samples showed smaller lamellae size (L_{lateral}) and larger long period (L_{ac}) compared with PLA, suggesting that, during drawing, more crystal fragmentation occurred and mesomorphic phase with extended-chain conformation formed for LCB-PLA due to the poor chain mobility.

Acknowledgements

This research was supported by National Natural Science Foundation of China (Grant No. 51303109), International Scientific and Technological Cooperation Project of Sichuan Province (Grant No. 2015HH0019) and Fundamental Research Funds for the Central Universities (Grant No. 2015SCU04A27).

References

- [1] E. Quero, A. J. Müller, F. Signori, Isothermal Cold - Crystallization of PLA/PBAT Blends With and Without the Addition of Acetyl Tributyl Citrate, *Macromol. Chem. Phys.* 213(2012) 36-48.
- [2] L. Yu, H. Liu, F. Xie, Effect of annealing and orientation on microstructures and mechanical properties of polylactic acid, *polym. Eng. Sci.* 48(2008) 634-641.
- [3] X. Yuan, A. F. T. Mak, K. W. Characterization of poly (L - lactic acid) fibers produced by melt spinning, *J. Appl. Polym. Sci.* 81(2001) 251-260.
- [4] B. Gupta, Revagade, N. Revagade, N. Anjum, Preparation of poly [lactic acid] fiber by dry - jet - wet - spinning. I. Influence of draw ratio on fiber properties, *J. Appl. Polym. Sci.* 100(2006) 1239-1246.
- [5] X. Zhao, L. Ye, Structure and properties of highly oriented polyoxymethylene produced by hot stretching, *Mat. Sci. Eng. A-Struct.* 528(2011) 4585-4591.
- [6] X. Zhao, L. Ye, Structure and properties of highly oriented polyoxymethylene/multi-walled carbon nanotube composites produced by hot stretching, *Compos. Sci. Technol.* 71(2011) 1367-1372.
- [7] J. Gu, Z. Lv, Y. Wu, Dielectric thermally conductive boron nitride/polyimide composites with outstanding thermal stabilities via in-situ polymerization-electrospinning-hot press method, *Compos. Part A: Appl. Sci. Manufac.* 2016.
- [8] J. Gu, Z. Lv, Y. Wu, Enhanced thermal conductivity of SiCp/PS composites by electrospinning-hot press technique, *Compos. Part A: Appl. Sci. Manufac.* 79(2015) 8-13.
- [9] S. Chokphoemphun, C. Hinthao, S. Eiamsa-ard, Thermal Performance in Circular Tube with Co/Counter-Twisted tapes, *Adv. Mater. Res. Trans Tech Publications*, 931(2014) 1198-1202.
- [10] X. Xu, Q. Yang, Wang, Y. Biodegradable electrospun poly (L-lactide) fibers containing antibacterial silver nanoparticles, *Eur. Polym. J.* 42(2006) 2081-2087.
- [11] Z. Li, L. Ye, X. Zhao, High orientation of long chain branched poly [lactic acid] with enhanced blood compatibility and bionic structure, *J. Biomed. Mater. Res. A.* 45(2016) 59-74.
- [12] Z. Li, X. Zhao, L. Ye, Fibrillation of chain branched poly [lactic acid] with improved blood compatibility and bionic structure. *Chem. Eng. J.* 279(2015) 767-776.
- [13] Z. Li, X. Zhao, L. Ye, Structure and blood compatibility of highly oriented poly [l-lactic acid] chain extended by ethylene glycol diglycidyl ether, *Polymer.* 56(2015) 523-534.
- [14] J. Gu, C. Liang, X. Zhao, Highly thermally conductive flame-retardant epoxy nanocomposites with reduced ignitability and excellent electrical conductivities, *Compos. Sci. Technol.* 139(2017) 83-89.
- [15] Z. Li, X. Zhao, L. Ye, Structure and blood compatibility of highly oriented PLA/MWNTs composites produced by solid hot drawing, *J. Biomater. Appl.* 97(2013) 15-26.
- [16] M. Bothe, T. Pretsch, Bidirectional actuation of a thermoplastic polyurethane elastomer, *J. MATER. CHEM. A.* 1(2013) 14491-14497

- [17] M. Jin, R. La, Y. Zhang, Stratiform β crystals in ultrahigh molecular weight polyethylene and β -nucleating agent-nucleated isotactic polypropylene at micro-injection molding condition, *Polym. Test.* 42(2015) 135-143.
- [18] M. Jin, K. Liu, H. Liu, Effects of polyolefin elastomer and β -nucleating agent on morphological evolution of isotactic polypropylene under an intensive shear rate, *Polym. Test.* 39(2014) 1-11.
- [19] C. Rotella, S. Tencé-Girault, M. Cloitre, Shear-Induced Orientation of Cocontinuous Nanostructured Polymer Blends, *Macromolecules.* 47(2014) 4805-4812.
- [20] V. A. Beloshenko, A. V. Voznyak, Y. Effect of simple shear induced orientation process on the morphology and properties of polyolefin/graphite nanoplates composites, *Compos. Sci. Technol.* 139(2017) 47-56.
- [21] Y. Tian, C. Zhu, J. Gong, Transition from shish-kebab to fibrillar crystals during ultra-high hot stretching of ultra-high molecular weight polyethylene fibers: In situ small and wide angle X-ray scattering studies, *Eur. Polym. J.* 73(2015) 127-136.
- [22] L. Peponi, I. Navarro-Baena, A. Sonseca, Synthesis and characterization of PCL-PLLA polyurethane with shape memory behavior, *Eur. Polym. J.* 49(2013) 893-903.
- [23] G. Liu, L. Zheng, X. Zhang, Critical Stress for Crystal Transition in Poly (butylene succinate)-Based Crystalline-Amorphous Multiblock Copolymers, *Macromolecules.* 47(2014) 7533-7539.
- [24] J. Liu, S. Zhang, L. Zhang, Uniaxial stretching of polylactide with different initial crystalline morphologies and temperature effect, *Eur. Polym. J.* 61(2014) 83-92.

Figure Captions

Fig. 1 Schematic diagram of PLA samples drawn through a die

Fig. 2 Schematic diagram of the die-drawing machine

Fig. 3 2D-WXRD patterns of (a) PLA and (b) LCB-PLA drawn under different drawing speed and die thickness of 0.55mm

Fig. 4 Orientation factors of PLA and LCB-PLA samples drawn under different drawing speed and die thickness of 0.55mm

Fig. 5 DSC curves of PLA and LCB-PLA samples drawn under different drawing speed and die thickness of 0.55mm

Fig. 6 Crystallinity of PLA and LCB-PLA samples drawn under different drawing speed and die thickness of 0.55mm

Fig. 7 2D-WXRD patterns of (a) PLA and (b) LCB-PLA drawn with different die thickness and drawing speed of 1000mm/min

Fig. 8 Orientation factor of PLA and LCB-PLA samples drawn with different die thickness and drawing speed of 1000mm/min

Fig. 9 DSC curves of PLA and LCB-PLA samples drawn with different die thickness and drawing speed of 1000mm/min

Fig. 10 Crystallinity of PLA and LCB-PLA samples drawn with different die thickness and drawing speed of 1000mm/min

Fig. 11 Mechanical properties of the oriented PLA and LCB-PLA samples (a) Samples drawn under a constant die thickness of 0.55mm and varying drawing speed (b) Samples drawn under a constant drawing speed of 1000mm/min and varying die thickness

Fig. 12 SEM images of fracture surface for PLA and LCB-PLA during die drawing (Drawing direction was indicated by the arrow)

Fig. 13 (a) The azimuthal scan of the lamellar peaks along q_y , (b) The one-dimensional scattering intensity distribution along q_x , (c) The average value of L_{lateral} and L_{ac} of PLA and LCB-PLA

Fig. 14 Proposed morphology evolution of PLA and LCB-PLA during solid die drawing process